

Chaos in Jahn-Teller Rattling

Takashi Hotta and Akira Shudo

Department of Physics, Tokyo Metropolitan University, Hachioji, Tokyo 192-0397, Japan

(Received July 25, 2021)

We unveil chaotic behavior hidden in the energy spectrum of a Jahn-Teller ion vibrating in a cubic anharmonic potential as a typical model for rattling in cage-structure materials. When we evaluate the nearest-neighbor level-spacing distribution $P(s)$ of eigenenergies of the present oscillator system, we observe the transition of $P(s)$ from the Poisson to the Wigner distribution with the increase of cubic anharmonicity, showing the occurrence of chaos in the anharmonic Jahn-Teller vibration. The energy scale of the chaotic region is specified from the analysis of $P(s)$ and we discuss a possible way to observe chaotic behavior in the experiment of specific heat. It is an intriguing possibility that chaos in nonlinear physics could be detected by a standard experiment in condensed matter physics.

KEYWORDS: Chaos, Rattling, Jahn-Teller vibration, Cubic anharmonicity

Recently, a peculiar magnetically robust heavy-electron phenomenon observed in Sm-based filled skutterudite compound¹⁾ has triggered active investigations on cage-structure compounds, in which a guest ion contained in a cage composed of relatively light atoms oscillates with large amplitude in an anharmonic potential. Such a local vibration with large amplitude is called *rattling* and exotic magnetism and superconductivity induced by rattling have attracted much attention in the research field of condensed matter physics. As easily understood from the above explanation, rattling is considered to be one of typical nonlinear phenomena, but unfortunately, such a viewpoint has not been recognized at all in the research field of nonlinear physics.

However, we emphasize an important point of contact between rattling phenomena and nonlinear physics through a concept of *chaos*. For nonlinear physicists, it will be quite natural to expect the appearance of chaos in the two-dimensional oscillator in a potential with plural numbers of minima. In fact, such a situation is expected to occur in cage-structure compounds, if we consider a Jahn-Teller ion vibrating in a cubic anharmonic potential,²⁾ in the course of the research of the Kondo effect with phonon origin.^{3–32)} It is worth to point out that such a cubic anharmonic term of Jahn-Teller vibration just indicates the Hénon-Heiles potential which has been discussed for the appearance of chaos in the early stage.³³⁾

Actually, apart from the rattling problem, the appearance of chaos in the vibronic state, i.e., the complicated electron-vibration coupled state, has been already pointed out by several groups.^{34–40)} However, we hit upon an idea that *chaos originates from anharmonic Jahn-Teller vibration*, not from the vibronic state composed of electron and anharmonic Jahn-Teller vibration. It is important to confirm that the origin of chaos exists in the anharmonic Jahn-Teller oscillator, since it will provide us a realistic model in condensed-matter physics for the research of chaos in nonlinear physics.

In this Letter, we clarify the chaotic property in anharmonic Jahn-Teller vibration. In order to confirm the appearance of chaos, we evaluate the nearest-neighbor level-spacing distribution $P(s)$, indicating that $P(s)$ changes from the Poisson to the Wigner distribution with the increase of cubic anharmonicity. We also discuss the energy region in which chaotic behavior occurs. In order to consider a possible way to detect

the chaotic behavior, we propose the measurement of specific heat in cage-structure materials. It is pointed out that the peak structure in the temperature dependence of specific heat could be a signal of chaotic behavior.

Let us consider a Jahn-Teller oscillator in an anharmonic potential. The Hamiltonian is given by⁴¹⁾

$$H = (P_1^2 + P_2^2)/(2M) + V(Q_1, Q_2), \quad (1)$$

where M is the reduced mass of Jahn-Teller oscillator, Q_1 and Q_2 denote normal coordinates of $(3z^2 - r^2)$ - and $(x^2 - y^2)$ -type Jahn-Teller oscillation, respectively, P_1 and P_2 indicate corresponding canonical momenta, and $V(Q_1, Q_2)$ is the potential for the Jahn-Teller oscillator. The potential is given by $V(Q_1, Q_2) = A(Q_1^2 + Q_2^2) + B(Q_1^3 - 3Q_1Q_2^2) + C(Q_1^2 + Q_2^2)^2$, where A is the quadratic term of the potential, while B and C denote the coefficients for third- and fourth-order anharmonic terms, respectively. As mentioned above, the third-order term is just the Hénon-Heiles potential.³³⁾ Note also that we include only the anharmonicity which maintains the cubic symmetry. Among the coefficients, A and C are taken as positive, while B is set as negative in this research.

In order to understand the properties of the potential, it is convenient to introduce the non-dimensional distortion as $q_1 = \sqrt{2M\omega}Q_1$ and $q_2 = \sqrt{2M\omega}Q_2$, where ω is the phonon energy given by $\omega = \sqrt{2A/M}$. By introducing q and θ through the relations of $q_1 = q \cos \theta$ and $q_2 = q \sin \theta$, we obtain V as

$$V(q, \theta) = \omega(q^2/4 + \beta q^3 \cos 3\theta/3 + \gamma q^4/8), \quad (2)$$

where non-dimensional anharmonicity parameters are defined by $\beta = 3B/[(2M)^{3/2}\omega^{5/2}]$ and $\gamma = 2C/(M^2\omega^3)$. Note that the energy scale of the potential is given by ω . Thus, in the following, we set the energy unit as $\omega = 1$.

In this potential, for $|\beta| \leq \sqrt{\gamma}$, there is a single minimum at $q=0$, while for $|\beta| > \sqrt{\gamma}$, there appear three minima for $q \neq 0$ in addition to the shallow minimum at $q=0$. In Fig. 1(a), we plot $V(q, \theta)$ vs. q for several values of θ for the case of $\beta = -2$ and $\gamma = 1$. Along the direction of $\theta = 0$, we find a deep minimum, while we find a saddle point along the direction of $\theta = \pi/3$. The potential structure is gradually changed with the increase of θ . In Fig. 1(b), we show the contour plot of the potential V for $\beta = -2$ and $\gamma = 1$. Here we find three minima along the directions of $\theta = 0, 2\pi/3,$ and $4\pi/3$, corresponding to $(3, -2)$

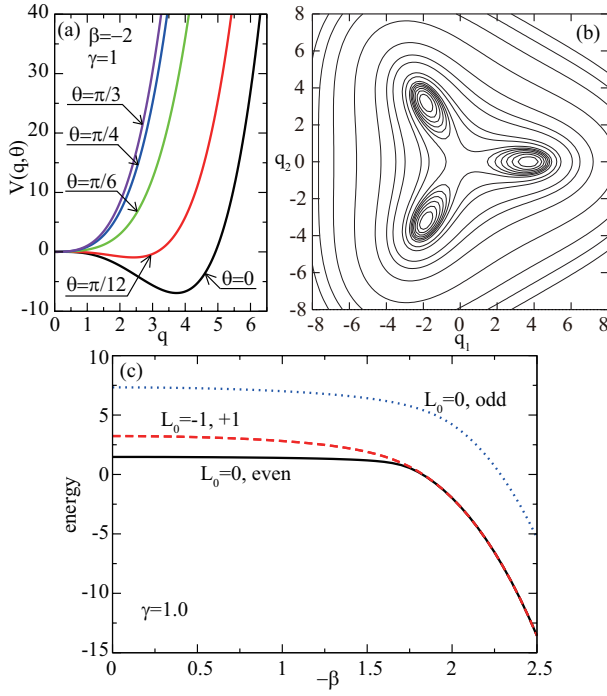


Fig. 1. (Color online) (a) Potential V vs. q along the directions of $\theta=0, \pi/12, \pi/6, \pi/4$, and $\pi/3$ for $\beta=-2$ and $\gamma=1$. (b) Contour plot of V on the q_1 - q_2 plane for $\beta=-2$ and $\gamma=1$. Here we draw the contour curves for $V=-6, -5, -4, -3, -2, -1, 0.5, 5, 10, 30, 50, 100, 250, 500$, and 750 . (c) Eigenenergies vs. $-\beta$ for the states of $L_0=0$ and ± 1 . Note that the states with $L_0=0$ is further classified into two types, specified by “even” and “odd”.

r^2), $(3x^2 - r^2)$ -, and $(3y^2 - r^2)$ -type Jahn-Teller distortions, respectively. Note that there still remains trigonal symmetry, as easily understood from the term of $\cos 3\theta$ in eq. (2), since we consider the cubic anharmonicity.

For the later discussion, here we define the potential depth V_0 as $V_0 = V(q_-, \theta = 0) - V(q_+, \theta = 0)$, where q_{\pm} denotes the position of extrema, given by $q_{\pm} = (-\beta \pm \sqrt{\beta^2 - \gamma})/\gamma$. Then, we obtain V_0 as

$$V_0 = 2|\beta|(\beta^2 - \gamma)^{3/2}/(3\gamma^3). \quad (3)$$

Note that V_0 is defined for $|\beta| \geq \sqrt{\gamma}$.

In order to discuss the local phonon state, it is necessary to perform the quantization procedure through the relations of $q_1 = a_1 + a_1^\dagger$ and $q_2 = a_2 + a_2^\dagger$, where a_1 and a_2 are annihilation operators of phonons for Jahn-Teller oscillations. In order to unveil the conserved quantities in the Hamiltonian H , it is useful to introduce the transformation of phonon operators as $a_{\pm} = (a_1 \pm ia_2)/\sqrt{2}$,⁴²⁾ where the sign in this equation intuitively indicates the rotational direction in the potential. With the use of these operators, the Hamiltonian is rewritten as

$$\begin{aligned} H = & a_+^\dagger a_+ + a_-^\dagger a_- + 1 \\ & + (\beta/3)[(a_+ + a_-^\dagger)^3 + (a_- + a_+^\dagger)^3] \\ & + (\gamma/2)(a_+^\dagger a_+ + a_-^\dagger a_- + 1 + a_+^\dagger a_-^\dagger + a_+ a_-)^2. \end{aligned} \quad (4)$$

Note again that the energy unit is set as $\omega=1$.

In order to diagonalize the Hamiltonian, we prepare the phonon basis $|L; n\rangle$, given by

$$|L; n\rangle = \begin{cases} |L + n, n\rangle & L \geq 0 \\ |n, n + |L|\rangle & L < 0. \end{cases} \quad (5)$$

where the phonon basis $|n_+, n_-\rangle$ is given by $|n_+, n_-\rangle = (1/\sqrt{n_+!n_-!})(a_+^\dagger)^{n_+}(a_-^\dagger)^{n_-}|0\rangle$ with the vacuum $|0\rangle$. In actual numerical calculations to solve the eigenvalue problem, the phonon basis $|L; n\rangle$ is truncated at a finite number N_{ph} and a maximum angular momentum L_{max} . In order to check the convergence, we have performed the numerical calculations for N_{ph} and L_{max} up to 250 and 125, respectively.

For $\beta=0$, we find that the quantum phonon state is labelled by the angular momentum L , given by $L = a_+^\dagger a_+ - a_-^\dagger a_-$. Note that L commutes with H for $\beta=0$. Thus, when we diagonalize the Hamiltonian for $\beta=0$, we prepare the phonon basis for a fixed value of L , since the states with different L are not mixed. When the potential has continuous rotational symmetry for $\beta=0$, the angular momentum should be the conserved quantity in the quantum mechanics.

When we include the effect of β , namely, cubic anharmonicity, the situation is changed. As easily understood from eq. (2), there occurs the trigonal term in the potential. In such a case, L is no longer the good quantum number, but there still exists conserved quantity concerning L . In order to clarify such a point, we express L as

$$L = 3\ell + L_0, \quad (6)$$

where L_0 takes the values of 0 and ± 1 . It is found that L_0 is the good quantum number.

The states with $L_0 = \pm 1$ is expressed by

$$|\Phi_k^{(\pm 1)}\rangle = \sum_{\ell, n} \varphi_{\ell, n}^{(k, \pm 1)} |3\ell \pm 1; n\rangle, \quad (7)$$

where $|\Phi_k^{(L_0)}\rangle$ denotes the k -th eigenstate characterized by quantum number L_0 and φ is the coefficient of the eigenstate. The corresponding eigenenergy is expressed by $E_k^{(L_0)}$.

Note that for the case of $L_0=0$, there exists extra conserved quantity of parity, concerning the change of $\ell \rightarrow -\ell$. It is simply understood from the fact that the bonding and anti-bonding states of $|3\ell; n\rangle$ and $|-3\ell; n\rangle$ are not mixed with each other. Then, the parity for the bonding (even) or anti-bonding (odd) state is another good quantum number. Note that the bonding state of $|3\ell; n\rangle + |-3\ell; n\rangle$ is mixed with $|0; n\rangle$, but the anti-bonding state $|3\ell; n\rangle - |-3\ell; n\rangle$ is not.

The state for $L_0=0$ with even parity is given by

$$\begin{aligned} |\Phi_k^{(0e)}\rangle = & \sum_n \varphi_{0, n}^{(k, 0e)} |0; n\rangle \\ & + \sum_{\ell > 0, n} \varphi_{\ell, n}^{(k, 0e)} (|3\ell; n\rangle + |-3\ell; n\rangle)/\sqrt{2}, \end{aligned} \quad (8)$$

while the state for $L_0=0$ with odd parity is given by

$$|\Phi_k^{(0o)}\rangle = \sum_{\ell > 0, n} \varphi_{\ell, n}^{(k, 0o)} (|3\ell; n\rangle - |-3\ell; n\rangle)/\sqrt{2}. \quad (9)$$

In short, we classify the eigenstates for the case of $\beta \neq 0$ into four groups with the labels of “+1”, “-1”, “0e”, and “0o”.

In Fig. 1(c), we plot $E_0^{(0e)}$, $E_0^{(\pm 1)}$, and $E_0^{(0o)}$, which denote the lowest eigenenergies of the groups of “0e”, “ ± 1 ”, and “0o”, respectively. We observe that the ground state is always given by $|\Phi_0^{(0e)}\rangle$ and the first excited state is doubly degenerate, given by $|\Phi_0^{(\pm 1)}\rangle$. Note that these three states seem to be almost degenerate in the region of $\beta < -1.7$. The state of $|\Phi_0^{(0o)}\rangle$ appears in the relatively high-energy region.

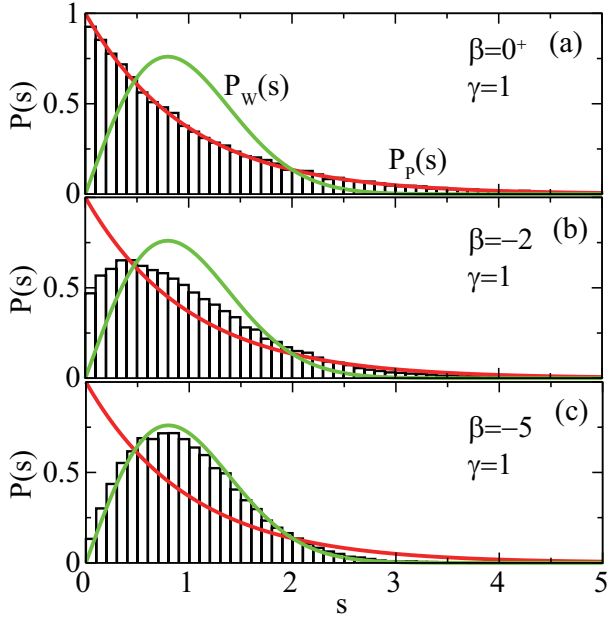


Fig. 2. (Color online) Nearest-neighbor level-spacing distribution $P(s)$ for (a) $\beta=0^+$, (b) $\beta=-2$, and (c) $\beta=-5$ for $\gamma=1$. Note that $P_P(s)$ and $P_W(s)$ denote the Poisson and Wigner distributions, respectively, given by $P_P(s)=e^{-s}$ and $P_W(s)=(\pi s/2)e^{-\pi s^2/4}$. To draw $P(s)$, we use the numerical data for $L_0=1$, but there is no significant difference in $P(s)$ even for $E_k^{(-1)}$ or $E_k^{(0e)}$.

The lowest-energy state of $L_0=0$ with even parity includes the significant contribution of $L=0$ and it corresponds to the zero-point oscillation. On the other hand, the state with $L_0=\pm 1$ has excitation with finite angular momentum. Around at $\beta \approx -1.7$, the zero-point energy is found to be less than the potential depth V_0 , suggesting that the oscillation states begin to be localized in the potential minima. In such a situation, the potential minima become deep and the quantum tunneling among potential minima is suppressed. Thus, the energy difference due to rotational motion becomes very small and the excitation energy is extremely reduced.

Now we explain a way to extract information on chaos from the energy spectrum.⁴³⁾ First we prepare the eigenenergies $\{E_k\}$ for each quantum number. Note that we cannot obtain correct distribution, if the eigenstates with different symmetry are mixed. Next we introduce the average counting function $\langle N(E) \rangle$, where $N(E)$ denotes the number of energy levels less than E , and perform the procedure of “unfolding” by the mapping $x_k = \langle N(E_k) \rangle$ with the unfolded level x_k . Then, we evaluate the distribution of nearest-neighbor level-spacing $P(s)\Delta s$ by counting the number of spacings satisfying $s < x_k - x_{k-1} < s + \Delta s$ with an appropriate mesh Δs .

In Fig. 2, we show $P(s)$ obtained from $E_k^{(+1)}$ with $\Delta s=0.1$ for $\beta=0^+$, -2 , and -5 . Here 0^+ indicates the infinitesimal small positive number. Note that there is no significant difference in the distribution $P(s)$, if we use the numerical data of $E_k^{(-1)}$ and $E_k^{(0e)}$. For $\beta=0^+$, we observe the Poisson distribution $P_P(s)=e^{-s}$, while for $\beta=-5$, we find the Wigner distribution $P_W(s)=(\pi s/2)e^{-\pi s^2/4}$. For $\beta=-2$, the mixture of $P_P(s)$ and $P_W(s)$ is observed. It is well known that when the classical system exhibits chaos, eigenenergies of the corresponding quantum system shows the Wigner distribution. Thus, we conclude that the chaotic behavior appears when we

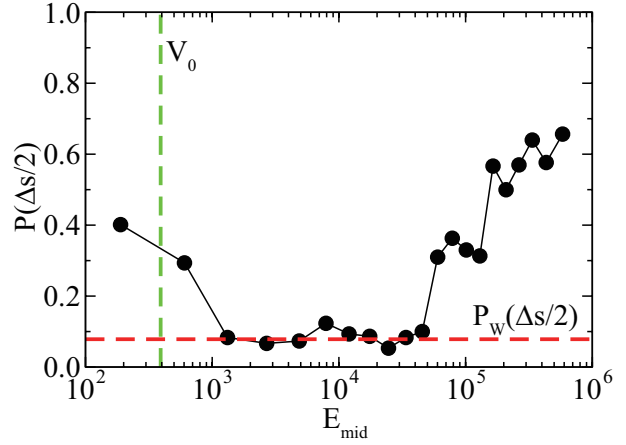


Fig. 3. (Color online) $P(\Delta s/2)$ vs. E_{mid} for $\beta=-5$ for $\gamma=1$. We set $\Delta s=0.1$ in the evaluation of $P(s)$. As for the meaning of E_{mid} , see the maintext. A vertical line denotes the potential depth V_0 , while a horizontal line indicates $P_W(\Delta s/2)$.

increase the cubic anharmonicity β . We also emphasize that the chaotic behavior observed in the vibronic state in the previous research should be considered to originate from chaos in the anharmonic Jahn-Teller vibration.

Here we have a naive question: In which energy region chaos predominates? In order to reply to this question, we divide the sequence of eigenenergies into several sectors and evaluate $P(s)$ of each sector. We consider the eigenenergies with $L_0=+1$ for $\beta=-5$ and $\gamma=1$, where $V_0=160\sqrt{6}=392$ from eq. (3). We prepare the following sequence of integer: $k_0=0$, $k_1=550$, and $k_j=3000 \times (j-1)$ for $j \geq 2$. Note that k_1 is determined so as to satisfy the relation of $E_{k_1}^{(+1)}=V_0$. We define the sector j including the eigenenergies from k_{j-1} to k_j . Then, for each sector j , we evaluate $P(s)$.

In Fig. 3, we plot $P(\Delta s/2)$ vs. E_{mid} for $\Delta s=0.1$, where E_{mid} indicates the energy just at the center of the sector j . The horizontal line denotes the value of $P_W(\Delta s/2)$. We find that for small E_{mid} comparable with V_0 , $P(\Delta s/2)$ is apparently larger than $P_W(\Delta s/2)$, suggesting that the chaotic nature is weak. This is understood from the fact that the oscillation is harmonic near the bottom of the potential well, since the potential is quadratic near the potential minimum. For large E_{mid} , we also observe that $P(\Delta s/2)$ significantly deviates from $P_W(\Delta s/2)$. For the energy region much larger than V_0 , the potential is dominated by the fourth-order term with q^4 and the system asymptotically approaches the integrable system, suggesting that the chaotic nature should disappear.

In the energy region for moderately larger than V_0 , we find the relation of $P(\Delta s/2) \approx P_W(\Delta s/2)$, although some deviations occur due to the statistical property. In one word, the result clearly defines the energy region with chaotic behavior. Namely, the chaotic nature comes from the eigenenergies between $a_L V_0$ and $a_H V_0$, where a_L is a number of the order of unity, while a_H is in the order of hundred. It seems natural that the energy of the chaotic region is related with the potential depth V_0 , but such energy region spreads over a few hundred times larger than V_0 . The width of the chaotic region is much larger than we have naively expected.

Now we discuss a possible way to detect the chaotic nature in observables. For the purpose we evaluate the specific heat

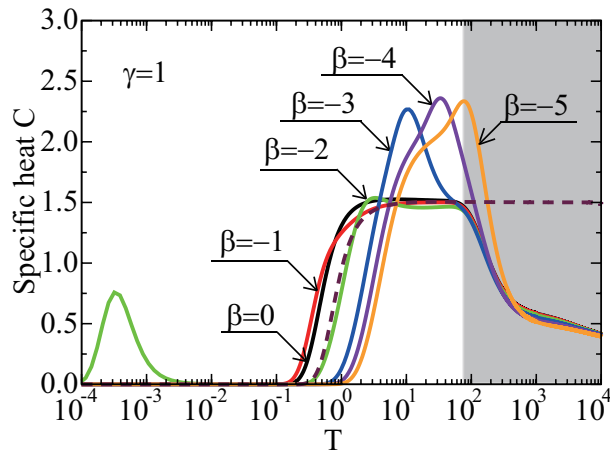


Fig. 4. (Color online) Specific heat C vs. T for several values of β with $\gamma=1$. The broken curve indicates the result of the one-dimensional anharmonic oscillator. A shaded square indicates a region in which numerical results for C did not converge satisfactorily in the present calculations.

C , given by $C = (\langle H^2 \rangle - \langle H \rangle^2) / T^2$, where T is a temperature and $\langle H^m \rangle = \sum_k e^{-E_k/T} E_k^m / Z$ with the partition function $Z = \sum_k e^{-E_k/T}$. Since the evaluation of C is done by the numerical calculation with the use of finite numbers of phonon bases, we should note that C may exhibit unphysical behavior at high temperatures.

In Fig. 4, we show the specific heat C vs. temperature T for several values of β . Note that the unit of C is k_B , which is set as unity.⁴¹⁾ For $\beta=0$ and -1 , C is increased rapidly around at $T \sim 1$ and it becomes almost a constant value, corresponding to the Dulong-Petit law. Note that the result agrees well with the broken curve of $2C_1$ in the high-temperature region, where C_1 denotes the specific heat of one-dimensional anharmonic oscillator in the potential of $V_1(q) = \omega(q^2/4 + q^4/8)$ with non-dimensional length q . At high enough temperatures, all the results should approach the broken curve, since the potential is dominated by the fourth-order term in the high-energy region. However, in the actual calculations with finite numbers of phonon bases, it is inevitable that C is deviated from the constant value at some temperature, as denoted by a shaded region in Fig. 4.

For $\beta=-2$, we find a hump at $T \sim 3.3$. At low temperatures, we find a Schottky peak determined by the first excitation energy $\Delta E = E_0^{(+1)} - E_0^{(0e)}$, which is the difference between lowest two curves in Fig. 1(c). Note that the Schottky peak cannot be observed for $\beta=0$ and -1 , since ΔE is larger than unity for both cases. On the other hand, for $\beta < -2$, the Schottky peak exists, but the peak position is smaller than 10^{-4} .

With the increase of $|\beta|$, the hump found in $\beta=-2$ grows and it eventually becomes the robust peak structure. The temperature at the peak T_p is found to be given by $T_p = 11, 33$, and 77 for $\beta = -3, -4$, and -5 , respectively. These values are well scaled by V_0 in eq. (3). For large values of $|\beta|$ such as $\beta = -4$ and -5 , we have carefully checked that the value of T_p converges even in the present numerical calculations, although it is difficult to reproduce the Dulong-Petit law consistent with $2C_1$ in the high-temperature region. Note, however, that we observe a shoulder in the position of $2C_1$ for $\beta = -3$.

From Figs. 3 and 4, the appearance of the peak structure with large width in the specific heat over the broken curve in

the high-temperature region seems to characterize the chaotic nature, since we intuitively consider that an entropy is expected to be enhanced due to uniform spreading of the eigenfunctions in the phase space for the energy region with chaotic behavior.^{44,45)} Here we note that C is related with the entropy S as $C = T(\partial S / \partial T)$, suggesting that C forms a peak when the entropy is rapidly increased with the increase of T . Thus, we deduce that the robust peak structure in the specific heat becomes a signal of the emergence of chaos.

In the experiments of cage-structure materials, the specific heat has been usually measured. In many cases, experimentalists have plotted the value of C/T^3 as a function of T , since the Debye specific heat is in proportion to T^3 at low temperatures. In the plot of C/T^3 vs. T , we obtain the peak structure corresponding to the characteristic frequency of the Einstein phonon for rattling. However, our proposal is to seek for the peak in C , not in C/T^3 , as the enhancement of C due to the chaotic nature of anharmonic Jahn-Teller vibration. A candidate material is cage-structure compound with off-center rattling such as clathrate. Note that we consider the specific heat in the temperature region higher than a room temperature.

In summary, we have clarified the chaotic nature of Jahn-Teller rattling. From the evaluation of $P(s)$, we have confirmed the occurrence of chaos in the anharmonic Jahn-Teller oscillation and the energy scale of the chaotic region. It has been emphasized that the chaotic behavior in the vibronic state of dynamical Jahn-Teller system originates from the anharmonic Jahn-Teller oscillation. We have proposed to observe the peak structure in the specific heat of cage-structure materials as a signal of the chaotic nature. It is a novel possibility to detect chaos in nonlinear physics by the standard experiment in condensed matter physics.

This work has been supported by JSPS KAKENHI Grant Numbers 25400405 and 24540379. The computation has been done using the facilities of the Supercomputer Center, the Institute for Solid State Physics, the University of Tokyo.

- 1) S. Sanada, Y. Aoki, H. Aoki, A. Tsuchiya, D. Kikuchi, H. Sugawara, and H. Sato: J. Phys. Soc. Jpn. **74** (2005) 246.
- 2) T. Hotta: arXiv:1405.7462.
- 3) J. Kondo: Physica B+C **84** (1976) 40.
- 4) J. Kondo: Physica B+C **84** (1976) 207.
- 5) K. Vladár and A. Zawadowski: Phys. Rev. B **28** (1983) 1564.
- 6) K. Vladár and A. Zawadowski: Phys. Rev. B **28** (1983) 1582.
- 7) K. Vladár and A. Zawadowski: Phys. Rev. B **28** (1983) 1596.
- 8) C. C. Yu and P. W. Anderson: Phys. Rev. B **29** (1984) 6165.
- 9) T. Matsuura and K. Miyake: J. Phys. Soc. Jpn. **55** (1986) 29.
- 10) T. Matsuura and K. Miyake: J. Phys. Soc. Jpn. **55** (1986) 610.
- 11) S. Yotsushashi, M. Kojima, H. Kusunose, and K. Miyake: J. Phys. Soc. Jpn. **74** (2005) 49.
- 12) K. Hattori, Y. Hirayama, and K. Miyake: J. Phys. Soc. Jpn. **74** (2005) 3306.
- 13) K. Hattori, Y. Hirayama, and K. Miyake: J. Phys. Soc. Jpn. **75** (2006) Suppl. 238.
- 14) K. Mitsumoto and Y. Ōno: Physica B **403** (2008) 859.
- 15) K. Mitsumoto and Y. Ōno: J. Phys. Soc. Jpn. **79** (2010) 054707.
- 16) T. Hotta: Phys. Rev. Lett. **96** (2006) 197201.
- 17) T. Hotta: J. Phys. Soc. Jpn. **76** (2007) 023705.
- 18) T. Hotta: J. Phys. Soc. Jpn. **76** (2007) 084702.
- 19) T. Hotta: Physica B **403** (2008) 1371.
- 20) T. Hotta: J. Phys. Soc. Jpn. **77** (2008) 103711.
- 21) T. Hotta: J. Phys. Soc. Jpn. **78** (2009) 073707.
- 22) S. Yashiki, S. Kirino, and K. Ueda: J. Phys. Soc. Jpn. **79** (2010) 093707.

- 23) S. Yashiki, S. Kirino, K. Hattori, and K. Ueda: J. Phys. Soc. Jpn. **80** (2011) 064701.
- 24) S. Yashiki and K. Ueda: J. Phys. Soc. Jpn. **80** (2011) 084717.
- 25) K. Hattori: Phys. Rev. B **85** (2012) 214411.
- 26) T. Hotta and K. Ueda: Phys. Rev. Lett. **108** (2012) 247214.
- 27) T. Fuse and Y. Ōno: J. Phys. Soc. Jpn. **79** (2010) 093702.
- 28) T. Fuse and Y. Ōno: J. Phys. Soc. Jpn. **80** (2011) SA136.
- 29) T. Fuse, Y. Ōno, and T. Hotta: J. Phys. Soc. Jpn. **81** (2012) 044701.
- 30) T. Fuse and T. Hotta: J. Phys.: Conf. Ser. **428** (2013) 012013.
- 31) T. Fuse and T. Hotta: J. Korean Phys. Soc. **62** (2013) 1874.
- 32) T. Fuse and T. Hotta: To appear in the Proceedings of SCES2013.
- 33) M. Hénon and C. Heiles: Astrophysical Journal **69** (1964) 73.
- 34) H. Köppel, W. Domcke, and L. S. Cederbaum: Adv. Chem. Phys. **57** (1984) 59.
- 35) R. S. Markiewicz: Phys. Rev. E **64** (2001) 026216.
- 36) H. Yamasaki, Y. Natsume, A. Terai, and K. Nakamura: Phys. Rev. E **68** (2003) 046201.
- 37) H. Yamasaki, Y. Natsume, A. Terai, and K. Nakamura: J. Phys. Soc. Jpn. **73** (2004) 1415.
- 38) E. Majerníková and S. Shpyrko: Phys. Rev. E **73** (2006) 057202.
- 39) E. Majerníková and S. Shpyrko: J. Molecular Structure **838** (2007) 22.
- 40) E. Majerníková and S. Shpyrko: J. Phys. A: Math. Theor. **44** (2011) 065101.
- 41) In this paper, we use such units as $\hbar=k_B=1$.
- 42) Y. Takada: Phys. Rev. B **61** (2000) 8631.
- 43) O. Bohigas: "Random matrix theories and chaotic dynamics", in *Chaos and Quantum Physics*, Les Houches, Session LII, 1989 (Eds. M. -J. Giannoni, A. Voros, and J. Zinn-Justin), pp. 87-199, Elsevier Sci. Publ., Amsterdam (1991).
- 44) M. V. Berry: J. Phys. A **10** (1977) 2083.
- 45) A. Voros: "Semi-classical ergodicity of quantum eigenstates in the Wigner representation", in *Stochastic Behavior in Classical and Quantum Hamiltonian Systems*, Lectures Notes in Physics Vol. 93 (Eds. G. Casati and J. Ford), pp. 326-333, Springer, Berlin (1979).